Open Archive Toulouse Archive Ouverte (OATAO)

To cite this version:

Al-Kattan, Ahmed and Girod Fullana, Sophie and Charvillat, Cédric and Ternet -Fontebasso, Hélène and Dufour, Pascal and Dexpert-Ghys, Jeannette and Santran, Véronique and Bordère, Julie and Pipy, Bernard and Bernad, José and Drouet, Christophe *Biomimetic nanocrystalline apatites: Emerging perspectives in cancer diagnosis and treatment.* (2012) International Journal of Pharmaceutics, vol. 423 . pp. 26-36. ISSN 0378-5173

Biomimetic nanocrystalline apatites: Emerging perspectives in cancer diagnosis and treatment

Ahmed Al-Kattan[a], Sophie Girod-Fullana[a], Cédric Charvillat[a], Hélène Ternet-Fontebasso[a], Pascal Dufour[a], Jeannette Dexpert-Ghys[b], Véronique Santran[c], Julie Bordère[c], Bernard Pipy[d], José Bernad[d], Christophe Drouet[a,*]

[a] *CIRIMAT Carnot Institute, UMR CNRS/INPT/UPS, University of Toulouse, France*
[b] *CEMES, University of Toulouse, France*
[c] *ICELLTIS, Verniolle, France*
[d] *UMR-MD3 EA2405, Université de Toulouse, France*

ABSTRACT

Nanocrystalline calcium phosphate apatites constitute the mineral part of hard tissues, and the synthesis of biomimetic analogs is now well-mastered at the lab-scale. Recent advances in the fine physico-chemical characterization of these phases enable one to envision original applications in the medical field along with a better understanding of the underlying chemistry and related pharmacological features. In this contribution, we specifically focused on applications of biomimetic apatites in the field of cancer diagnosis or treatment. We first report on the production and first biological evaluations (cytotoxicity, pro-inflammatory potential, internalization by ZR-75-1 breast cancer cells) of individualized luminescent nanoparticles based on Eu-doped apatites, eventually associated with folic acid, for medical imaging purposes. We then detail, in a first approach, the preparation of tridimensional constructs associating nanocrystalline apatite aqueous gels and drug-loaded pectin microspheres. Sustained releases of a fluorescein analog (erythrosin) used as model molecule were obtained over 7 days, in comparison with the ceramic or microsphere reference compounds. Such systems could constitute original bone-filling materials for *in situ* delivery of anticancer drugs.

1. Introduction

The setup and development of fine-tuned diagnosis devices and biomimetic drug delivery systems appear today as major challenges in modern medicine, and specifically in oncology.

Nanocrystalline calcium phosphate apatites, responding to the general chemical formula $Ca_{10-x}(PO_4)_{6-x}(HPO_4)_x(OH)_{2-x}$ ($0 \leq x \leq 2$), can be seen as promising candidates for the preparation of nano-biotechnological devices (Rey et al., 2007; Roveri et al., 2008). Indeed, they fully mimic the composition and structural features of bone mineral, which confers them a biocompatible character. Also, they do not originate from biological sources thus eliminating immunological or ethical issues (as well as a poor reproducibility in compound characteristics). Their physico-chemical characteristics and surface state have been investigated in details, as well as their potentialities in bone regeneration appli-

cations (see for example Rey et al., 2007, 2009; LeGeros, 2008; Autefage et al., 2009). In contrast to well-crystallized micron-sized hydroxyapatite, nanocrystalline apatitic systems exhibit a high surface reactivity and their preparation is now mastered at the lab-scale (Drouet et al., 2009). Also, recent results have shown the possibility to retain the advantageous physico-chemical features of apatite nanocrystals by using soft processing routes (e.g. Grossin et al., 2010).

In this view, two domains of interest for apatite-based systems can be more specifically considered: the preparation of individualized nanoparticulate systems and the elaboration of tridimensional biomimetic constructs.

The development of nanoparticle-based systems in medicine has been widely described. Examples of individualized nanoparticulate systems currently investigated include metal or metal oxide nanoparticles (e.g. gold, magnetite, gadolinium oxide), semiconductors (e.g. quantum dots), polymeric nanoparticles or nanocapsules, liposomes, etc. (Bruchez et al., 1998; Parak et al., 2003; Ow et al., 2005; Fizet et al., 2009). These nano-systems may be used as circulating entities in body fluids, associated with limited recognition by the reticulo-endothelial system (Moghimi et al., 2001; Moghimi and Bonnemain, 1999; Couvreur et al., 2006),

* Corresponding author at: CIRIMAT Carnot Institute, ENSIACET, 4 allee Emile Monso, 31030 Toulouse cedex 4, France. Tel.: +33 5 34 32 34 11; fax: +33 5 34 32 34 99.

E-mail address: christophe.drouet@ensiacet.fr (C. Drouet).

in view of specific cell addressing and internalization (Schroeder et al., 2007), possibly with the help of a cell-targeting agent such as folic acid (FA). The use of apatites for cellular drug delivery (e.g. for nonviral transfection applications) or medical imaging has also lately raised interest in the scientific community due to the possibility to functionalize the surface of biomimetic apatite nanocrystals with varying molecules of interest (Mondejar et al., 2007; Bouladjine et al., 2009; Saha et al., 2009; Al-Kattan et al., 2010). Very recently, we showed the possibility to prepare colloidal apatite-based suspensions from ionic salts for the elaboration of luminescent nanoparticles (Al-Kattan et al., 2010), opening new perspectives in medical diagnosis.

The association of apatitic tridimensional constructs with biologically relevant ions or drugs, including anticancer agents, has also been pointed out (Lebugle et al., 2002; Barroug et al., 2004; Josse et al., 2005; Gautier et al., 2010; Autefage et al., 2009; Roveri et al., 2008; Drouet et al., 2008). The possibility to control the nanocrystalline character of such systems makes it possible to take advantage of the surface properties and enhanced bioactivity (Cazalbou et al., 2005; Rey et al., 2007; Tran et al., 2009). Also, new processing routes avoiding high-temperature sintering steps open new perspectives in elaborating drug-loaded scaffolds, as low-temperature processes are needed to retain the active structure of numerous drugs. In the absence of specific apatite–drug interaction, the simple incorporation of the drug within the apatitic matrix often leads to uncontrolled burst release. In this context, including drug-loaded polymer microparticles into ceramics could be a way to improve drug release properties. Polymer microparticles incorporated into calcium phosphate cements (whose final composition is apatitic) have already been described and showed interesting delayed release properties (Ruhe et al., 2005; Habraken et al., 2008; Girod-Fullana et al., 2010). However, despite a controlled drug release, this type of formulations bears potential drawbacks due in particular to the usual exothermic effect and/or pH change occurring upon cement hardening (which could prove to be problematic for some drugs) and to the modification of the cement hardening kinetics as a function of the amount of associated microspheres.

Taking into account the preceding statements, we investigated in the present work the potentialities of biomimetic nanocrystalline apatite-based systems specifically in view of cancer-related applications: either (i) for intracellular medical imaging (cancer diagnosis) or (ii) in view of local drug delivery (e.g. anticancer drug) in cancerous bone tissue.

In the first case, we focused on the above-mentioned luminescent apatite colloids. We proved the possibility to functionalize the surface of the apatite nanoparticles with folic acid, or "FA" (a potential cell-targeting agent), and we evaluated (i) their cytotoxicity on different cell types: breast cancer cells (ZR-75-1) and adipose stem cells from breast (AMSC) which are involved in progression of closed tumor cells, (ii) their pro-inflammatory potential (by following interactions with Human monocytes/macrophages), and (iii) their capacity to be internalized by ZR-75-1 breast cancer cells. Such biocompatible systems then show promise as biocompatible luminescent nanoprobes.

In the second case, we present a novel approach for the preparation of polymer/apatite composites, involving the progressive mild drying of an aqueous biomimetic apatite gel containing drug-loaded microspheres. This study explores the feasibility of incorporating low methoxy amidated pectin (LMAP) microspheres into a nanocrystalline apatite ceramic, with the aim to study the influence of pectin microspheres on the ceramic crystalline structure and to evaluate the composite drug release ability. To do so, varying LMAP incorporation ratios, up to 18% (w/w), were tested and erythrosin (a red fluorescent dye) was chosen as model drug to be released.

2. Materials and methods

2.1. Samples preparation

The apatite colloids prepared in this work were obtained by applying the experimental protocol that we reported previously (Al-Kattan et al., 2010). A constant europium doping rate corresponding to the final molar ratio $Eu/(Ca + Eu) = 2\%$ was used here. Briefly, the nanocrystalline apatite precipitation was carried out in deionized water, at room temperature and pH 9.5, from a mixture of calcium nitrate, europium nitrate and ammonium hydrogenphosphate, with the starting molar ratio $(Ca + Eu)/P = 3$, and in the presence of a phospholipid moiety: 2-aminoethylphosphate (denoted "AEP") playing the role of biocompatible stabilizing agent through electrostatic interparticle repulsive effects (Bouladjine et al., 2009). After precipitation, the suspensions were aged at $100\,°C$ for 16 h. The starting $AEP/(Ca + Eu)$ molar ratio was fixed to 1. The fluid colloids obtained after aging were then purified by dialysis in water (cellulose membrane, cutoff 6000–8000 Da). The pH of the colloids could then be adjusted to physiological value by addition of sodium hexametaphosphate, prior to biological applications. In the case of syntheses performed in the presence of folic acid (vitamin B9 or "FA"), the latter was added either in the reacting medium before or after the aging step, typically at a concentration of 0.45 mM.

The preparation of the pectin–apatite composite samples involved two successive steps: the preparation of erythrosin-loaded pectin microspheres (ERY-LMAP), and the association of LMAP microspheres with nanocrystalline apatite gel. In this work, we used low-methoxy amidated pectins (LMAP) with degrees of esterification and amidation of 30% and 19%, respectively, and an average molecular weight of 228 000 Da, as supplied by CPKelco (Denmark). LMAP microspheres were prepared as follows: 3% (w/v) pectin were dispersed into erythrosin B solutions in phosphate buffer pH 8. ERY-LMAP microspheres were produced by ionotropic gelation using an electrostatic bead generator (Inotech encapsulator IE 50 R, Switzerland) equipped with a syringe pump and a $300\,\mu m$ nozzle. The pectin solutions were dropped into a solution of calcium chloride at 500 mM (cross-linking solution) under continuous agitation. The gelled microspheres, instantaneously formed, were allowed to cure in the cross-linking solution for 24 h. Then they were separated by filtration, washed with deionized water, dehydrated in a graded series of ethanol, and dried for 48 h at $37\,°C$.

The preparation of the pectin–apatite biocomposites was then carried out in the shape of disks (final dimensions: 18 mm diameter, 5 mm height). In a typical procedure, dried LMAP microspheres were dispersed, in varying amounts (50, 100, 200 and 300 mg), into a 100 ml solution of calcium nitrate $Ca(NO_3)_2 \cdot 4H_2O$ at a concentration of 160 g/l. A 50 ml ammonium hydrogenphosphate $(NH_4)_2HPO_4$ solution at 70 g/l was then prepared and adjusted to pH 10.5 by addition of 5 ml of ammonia, and dropped into the calcium–pectin suspension under continuous stirring. After 1 min of reaction, the obtained gel was filtered and washed with deionized water. This pectin-loaded gel was finally introduced into cylindrical moulds and pressed until total evacuation of air bubbles. The lids of the mould were removed and the paste was allowed to dry, in varying temperatures, during 4 days.

2.2. Physico-chemical characterizations

Calcium and europium contents were assessed by induced coupled plasma atomic emission spectroscopy, ICP-AES (relative uncertainty 3%). The amount of mineral phosphate in the samples was determined by colorimetry at $\lambda = 460\,nm$ using the yellow phospho-vanado-molybdenum complex (relative uncer-

tainty 0.5%). The AEP content in apatite colloids was drawn from nitrogen microanalysis (relative uncertainty 0.4%).

The apatitic crystallographic structure in the samples was checked, after freeze-drying, by powder X-ray diffraction (XRD) using a CPS 120 INEL diffractometer and the K_α cobalt radiation ($\lambda = 1.79002$ Å). Fourier transform infrared (FTIR) analyses were performed on a Nicolet 5700 spectrometer, in the wavenumber range of 400–4000 cm^{-1} with a resolution of 4 cm^{-1}.

The size and morphology of the samples were followed, depending on the size range of the samples, either by optical microscopy, by scanning electron microscopy (SEM) using a JEOL scanning electron microscope (JSM-6400F) at 15 kV, or by transmission electron microscopy (TEM) on a JEOL JEM-1011 set at 100 keV.

The particle size of apatite colloids (hydrodynamic diameter) was determined by dynamic light scattering (DLS) using a Nanosizer ZS apparatus from Malvern Instruments ($\lambda = 630$ nm). The dispersion of the data points is estimated to 0.5%. Zeta potential measurements were also carried out using this apparatus. The LMAP microspheres size distributions were measured using a laser particle sizer (Mastersizer 2000; Malvern, UK) based on a laser light-scattering technique. Each sample was measured in triplicate. The weight average of volume distribution ($D[4;3]$) was used to describe the particle size.

Microsphere swelling ratio was evaluated by weighing, and calculated according to Eq. (1):

$$SR = \left[\frac{W_t - W_0}{W_0} \right] \times 100 \tag{1}$$

where W_t is the microspheres weight at the given time point and W_0 the initial weight of the dry microspheres. Each experiment was performed in triplicate.

The luminescence properties of the colloids were investigated using a Horiba Jobin Yvon Fluorolog 3-11 spectrofluorometer equipped with a 450 W xenon lamp. Excitation and emission were measured at room temperature directly on the dialyzed colloidal suspensions. Excitation spectra were recorded between 350 and 600 nm, monitoring the $^5D_0 \rightarrow {}^7F_2$ emission of Eu^{3+} at $\lambda_{em} = 612$ nm (spectral bandwidth = 2 nm). Emission spectra were recorded in the 500–700 nm range, with a spectral bandwidth of 1 nm, under selected excitation in the $^7F_0 \rightarrow {}^5L_6$ transition of Eu^{3+} at $\lambda_{ex} = 392.8$ nm or in the $^7F_0 \rightarrow {}^5D_2$ transition at $\lambda_{ex} = 464.2$ nm. The transient characteristics of the emitting level $^5D_0$ of Eu^{3+} were investigated with the phosphorimeter FL-1040, equipped with a UV xenon flash tube. Emission decays were analyzed at chosen λ_{ex} and λ_{em} on a time interval of 3.5 ms. The time resolution imposed by the apparatus in the experimental conditions employed is 30 μs.

Fluorescent confocal microscopy was used to characterize LMAP microspheres after release. An argon 488 nm laser was used for excitation of erythrosin; the emission light between 505 and 530 nm was detected. Using a Zeiss 510 confocal microscope, optical sections of 46.8 μm thick through the microspheres were taken.

For the LMAP–apatite composite systems, drug loading and encapsulation efficiency were determined after complete degradation of LMAP microspheres in pH 8 phosphate buffer. They were calculated according to Eqs. (2) and (3), respectively:

Drug loading

$$= \left[\frac{AQ}{\text{total weight of microspheres by batch} - AQ} \right] \times 100 \tag{2}$$

Encapsulation efficiency (drug entrapment ability in %)

$$= \left(\frac{AQ}{TQ} \right) \times 100 \tag{3}$$

in which AQ is the actual quantity of drug present in the matrices (drug content) and TQ the theoretical quantity of drug (initial erythrosin B loading dose during microspheres preparation).

Erythrosin B release from microspheres, ceramics alone, and composites under *in vitro* conditions was performed in SBF pH 7.25 (prepared according to Kokubo and Takadama, 2006) at 37 °C. Standard methods of release experiments in pharmacopoeias are hardly suitable for multi-particulate dosage forms due to the large volumes of the vessels; a modified alternative method, proposed by research groups working on multi-particulate dosage forms for colon delivery was used (Atyabi et al., 2005). Briefly, composites (containing ERY-LMAP microspheres at a weight ratio of 6% and 9%, respectively) or ceramic specimens (accurate weight of approximately 2.80 g) or ERY-LMAP microspheres (accurate weight of approximately 100 mg) were placed in test tubes containing 10 ml of SBF pH 7.25, at 37 °C under agitation at 100 rpm. Erythrosin B was assayed by spectrophotometry (Perkin Elmer, USA) at 527 nm, in triplicate, at various time intervals up to 7 days. Cumulated released amounts (in percentage of the initial amounts) were plotted versus time. Each *in vitro* release study was performed three times. All the studies were performed under sink conditions for erythrosin B.

2.3. Biological assessments

2.3.1. Cytotoxicity evaluation for apatite-based colloidal nanoparticles

The cytotoxicity of the colloids, relatively to two cell types: human breast cancer cells ZR-75-1 and adipose tissue mesenchymal stem cells (AMSC), was evaluated by way of MTT tests performed by the ICELLTIS Company (Verniolle, France). In these tests, cell viability is determined on the basis of mitochondrial activity which leads to a quantifiable emission of light after exposure with the MTT reactant (3-[4,5-dimethylthiazol-2yl]-2,5-diphenyltetrazolium bromide).

In preparation of these tests, the cells were cultivated in humidified atmosphere with 5% CO$_2$ at 37 °C in Dulbecco's Modified Eagle's Medium (DMEM) supplemented with 10% fetal bovine serum and 1% antibiotics (penicillin/streptomycin). The cells were then placed in 96-well culture plates (30 000 cells per well) and each test was run in triplicate. After 24 h of preliminary incubation, the culture medium was replaced by fresh DMEM (exempt of phenol red) and the MTT tests were initiated.

Cell viability was assessed for varying contact times between the colloidal nanoparticles and the cells ranging between 1 and 7 days. Additionally, 5 different concentrations of nanoparticles in the culture medium were tested: 0, 0.1, 1, 2, 5 and 10 mg/ml. For each MTT test, 50 μl of MTT reactant (5 mg/ml) were added to each well and the cells were further incubated for 4 h at 37 °C for completing the reaction. Finally, the culture medium was replaced by a solubilization solution (H$_2$O 66%, DMF 20%, SDS 5%, Triton X100, at pH 7) overnight and measurement of the light absorption at 570 nm was carried out, as a measure of cell viability.

2.3.2. Evaluation of the pro-inflammatory potential of apatite-based colloids – interaction with Human monocytes

Macrophages and their precursors, monocytes, are essential cells of the immunological system, intended to mediate the inflammatory response to foreign substances such as nanoparticles. These cells are in particular activated by inflammatory signals, conducing to an increased capacity to release pro-inflammatory and cytotoxic mediators such as Reactive Oxygen Intermediates, or "ROI" (Laskin and Laskin, 2001). The measure of the amount of produced ROI was thus used in this work to evaluate the intrinsic pro-inflammatory potential of the apatite colloidal nanoparticles that we prepared.

For these measurements Human peripheral blood mononuclear cells were isolated from the blood of healthy volunteers

by a density gradient centrifugation method on Lymphoprep (Abcys). Monocytes were isolated by adherence to plastic for 2 h in Macrophage-Serum Free Medium (M-SFM) (Gibco Invitrogen) at 37 °C, 5% CO_2.

The monocytes were plated in 96-well Falcon plates (3×10^5 monocytes/well). The oxygen dependent respiratory burst of monocytes was measured by chemiluminescence as previously described (Lefevre et al., 2010) in the presence of 5-amino-2,3-dihydro-1,4-phthalazinedione (luminol) using thermostatically (37 °C) controlled luminometer (Wallac 1420 Victor2). The luminol detects both reactive oxygen and nitrogen intermediates ($O_2^{\bullet-}$, $ONOO^-$, $OH^\bullet$). The generation of chemoluminescence was monitored continuously for 1 h after incubation of the cells with luminol (66 mM) and after colloids challenge at various concentrations (1.2, 12, 60 and 120 μg/ml). The measurements was realized in triplicate. The negative control was based on experiments carried out in the absence of nanoparticles. Statistical analysis was performed using the area under the curve expressed in counts × seconds.

2.3.3. Evaluation of the internalization of colloidal apatite nanoparticles by ZR-75-1 breast cancer cells

The possible internalization of apatite colloidal nanoparticles by cancer cells was checked on ZR-75-1 breast cancer cells, for a concentration of nanoparticles in the culture medium of 1.5 mg/ml. A negative control was carried out without nanoparticles.

These tests, realized in triplicate, were carried out by the ICELLTIS Company (Verniolle, France). 24 h after seeding, the colloid was added to the cells during 24 h. Then, after washing with PBS buffer, the cells were counted and centrifuged. The residual pellets were dissolved in HCl 37% and incubated for 30 min in view of quantification of the intracellular Eu and Ca contents by ICP-AES (analyses preformed by the MARION TECHNOLOGIES Company, Verniolle, France).

3. Results and discussion

3.1. Biomimetic apatite colloids in view of cancer-related medical imaging

3.1.1. Physico-chemical aspects

The colloidal apatite-based suspensions prepared in this work, in the presence of 2-aminoethylphosphate (AEP), correspond to an experimental europium content of 2 at.% relative to calcium as indicated by ICP-AEP evaluations. Also, the (Ca + Eu)/P and AEP/apatite molar ratios were found to be close to 1.60 and 0.63, respectively. The possibility to substitute some Ca^{2+} ions by Eu^{3+} in the apatite structure has indeed been already shown (e.g. Boyer et al., 2000).

XRD analysis carried out on a typical dialyzed and freeze-dried colloid (Fig. 1a) confirmed the apatitic nature of the crystallized particles prepared, with no detectable traces of secondary phases. FTIR spectral features (Fig. 1b) corroborated these findings. The presence of AEP molecules associated with the apatite phase was indicated by the presence of an absorption band at 754 cm^{-1}, linked to P–O(C) libration in systems such as Ca(AEP)$_2$ involving a close interaction between AEP and Ca^{2+} ions, as was discussed in our previous works (Bouladjine et al., 2009; Al-Kattan et al., 2010). Moreover, in these studies the adsorption of the AEP molecules on the surface of apatite nanoparticles was evidenced, explaining the colloidal stabilization effect by way of electrostatic repulsions among adjacent particles through the ammonium –NH$_3^+$ terminal groups of the grafted AEP molecules. The zeta potential of the colloids prepared in the present work was found to be close to +12 ± 3 mV, and this positive value is indeed in good agreement with this statement. Although this zeta potential measure may appear rather low in absolute value,
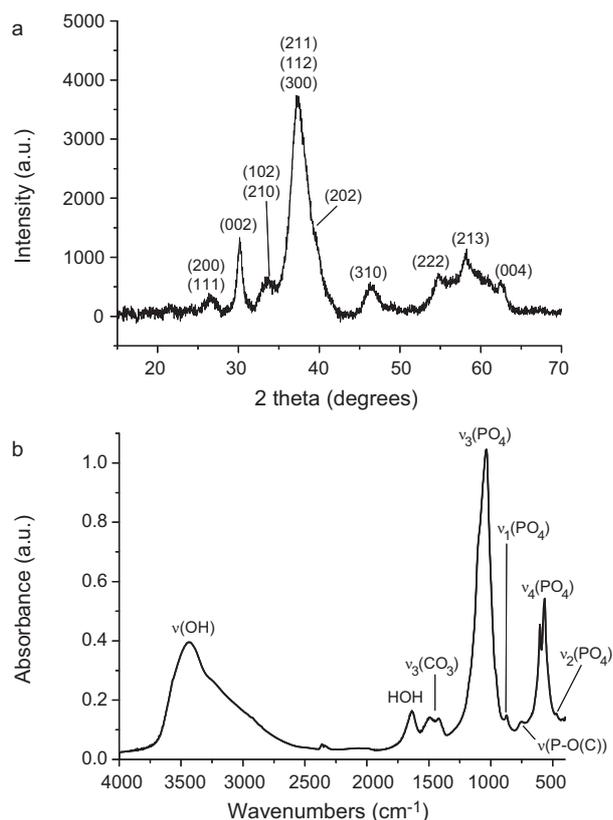

Fig. 1. (a) XRD patterns and (b) FTIR spectra for apatite colloidal nanoparticles.

the colloidal stability could be assessed macroscopically (by optical observations) and the as-synthesized colloids did not undergo sedimentation. However, it should be noted here that a complete follow-up of the stability over time of such colloidal suspensions was out of the scope of the present study, and will be regarded in a detailed upcoming work.

TEM observations of such colloids (Fig. 2a) pointed out the homogeneous ellipsoidal morphology of the nanoparticles, with a mean length of the order of 25 ± 3 nm and a mean width of 7 ± 1 nm (as determined from image processing carried out with the ImageJ software). DLS measurements (Fig. 2b) confirmed the nanometer-scale dimensions of the particles, with a unimodal size distribution centered around 30 nm.

The luminescence properties of the colloids were also investigated (Fig. 3). Excitation spectra recorded by monitoring the red luminescence intensity or Eu^{3+} at 612 nm (main emission line) showed two main emission peaks upon excitation at 392.8 nm (major peak) and 464.2 nm corresponding, respectively, to the $^7F_0 \rightarrow {}^5L_6$ and $^7F_0 \rightarrow {}^5D_2$ intraconfigurational transitions. These low-energy excitation domains (as compared for example to systems excitable solely under UV wavelengths) thus enable one to envision the investigation of biological material while preventing a premature deterioration. Luminescence emission spectra recorded under excitation at 392.8 nm indicated the presence of three main domains in the ranges 575–580 nm, 583–603 nm, and 605–627 nm, corresponding, respectively, to the transitions from the $^5D_0$ excited state to the $^7F_0$, $^7F_1$ and $^7F_2$ states of Eu^{3+}.

The luminescence decay time τ (defined as the time for which $I(\tau) = I_0/\exp(1)$) of the europium $^5D_0$ level was also measured, reaching 0.74 ± 0.03 ms. This value of the order of a millisecond is remarkably lager than the typical decay times for the auto-fluorescence of biological tissues thus adding to the potential
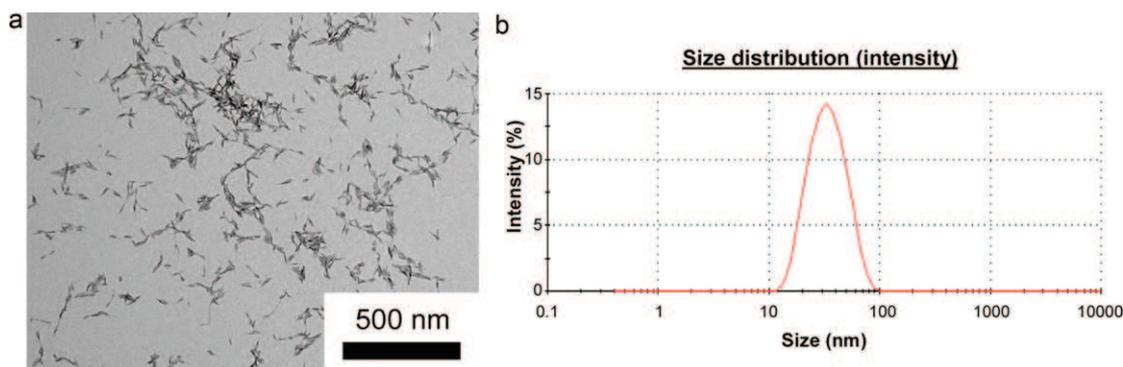
Fig. 2. (a) TEM micrograph and (b) DLS data for apatite colloidal nanoparticles.

interest of such luminescent nano-systems as biologically oriented nanoprobes.

The above data stress that Eu-doped apatite colloids can be prepared, in aqueous medium, and that they may be considered for applications in the field of medical imaging, in particular due (i) to the biocompatible nature of their constituents (biomimetic apatite and phospholipid moiety), (ii) to the nanometer-scale dimensions of the particles (typically ~30 nm) aiming at facilitating internalization by cells, (iii) to the possibility to excite these systems under (low-energy) visible or close-to-visible light domains, and (iii) to the long luminescence lifetime as compared to the autofluorescence of biological tissues.

An interesting aspect to address when nanoparticles–cells interactions are envisioned concerns the possibility to target a specific type of cells (or tissue) so as to develop "intelligent" diagnosis or therapeutic tools. In this context, several potential targeting agents can be envisaged depending on several parameters such as the type of pathology, the nature of the targeted cells, the degree of specificity of the targeting agent, etc.

Folic acid (vitamin B9 or "FA") is an example of targeting agent that has led to numerous studies worldwide in the field of oncology. Indeed, various works have shown that certain types of cancer cells (e.g. some ovarian or breast cancer cells for instance) were over-expressing on their membrane some specific folate receptors FR (e.g. Antony, 1992; Parker et al., 2005) which exhibit a high affinity for the folic acid molecule (about 100 000 times greater than that of the reduced folate receptors that are usually present on the surface of normal cells, (Spinella et al., 1995)). Another interesting feature is that folic-acid-mediated endocytosis was generally observed for

FA-functionalized nano-systems, right after recognition of FA by the FR receptors (Kamen et al., 1988).

In the present work, we thus focused on the physico-chemical feasibility of FA association on our apatite colloidal nanoparticles. Taking into account the two carboxylate groups of the glutamic acid-like head of the FA molecule, we thus suspected a favorable adsorption of FA molecules on the surface of apatite nanocrystals by way of Ca^{2+} accessible surface ions.

Our attempts to functionalize the surface of apatite colloidal nanoparticles by introducing FA in the reacting mixture (either before or after the aging step), at a typical concentration of 0.45 mmol/l, proved to be successful. Apart from a clear yellow color for the colloids (due to the presence of FA) the main physico-chemical characteristics of the nanoparticles were retained. In particular, no secondary crystallized phase was detected from XRD analyses which were similar to the FA-free samples, and the 754 cm^{-1} IR absorption band assignable to the presence of AEP molecules was conserved. The DLS- and TEM-derived mean particle size (43 ± 5 nm) remained also essentially unchanged. C, H, N elemental analyses on freeze-dried nanoparticles led to an FA content of 1.03 mg/100 mg of dried suspension. This low concentration in FA did not allow us to detect its presence by FTIR spectroscopy; however the use of greater FA concentrations (4–40 times greater) led to the appearance of absorption bands characteristic of calcium folate in the region 940–1800 cm^{-1}, next to the bands characteristic of the apatite phase, in particular at 1590 and 1396 cm^{-1} (not shown for the sake of brevity). On the contrary, the typical bands of free folic acid (especially at 1671 cm^{-1}) were not seen. These data evidenced the existence of FA–Ca^{2+} interactions and thus confirm the physical attachment of FA molecules on the nanoparticles surface, as initially planned.

Luminescence spectra on the FA-functionalized colloids were then recorded as previously, after excitation at 392.8 nm (see Fig. 3). As for the FA-free suspensions, the spectra were characteristic of the Eu^{3+} emitting centers despite a baseline drift due to the presence of the grafted FA molecules. The luminescence decay time was also determined ($\tau_{FA} = 0.74$ ms) and was found to be unmodified by the presence of FA.

3.1.2. Cytotoxicity assessments

For a concentration of nanoparticles in the culture medium between 0 and 1 mg/ml, the tests carried out on AMSC cells (see Fig. 4 for FA-functionalized colloids) indicated a cell viability close to 100%, whatever the incubation time between 1 and 7 days. These results were found to be independent on the presence or absence of FA on the nanoparticles. For greater concentrations in nanoparticles, the cell viability started to decline thus enabling to consider
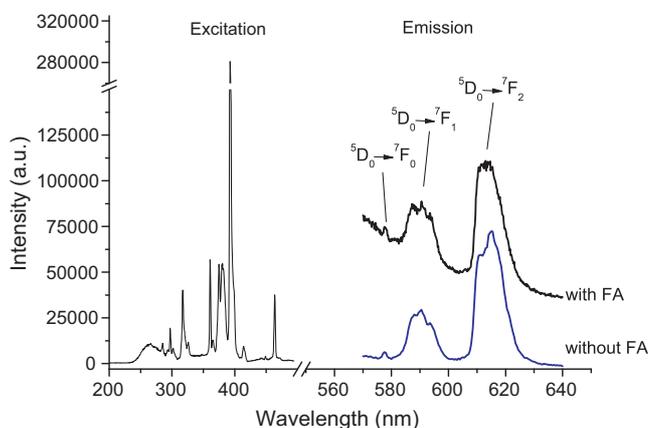

Fig. 3. Luminescence properties of apatite colloidal nanoparticles: excitation and emission (with or without FA functionalization) spectral features.

AMSC cells - <u>presence</u> of FA

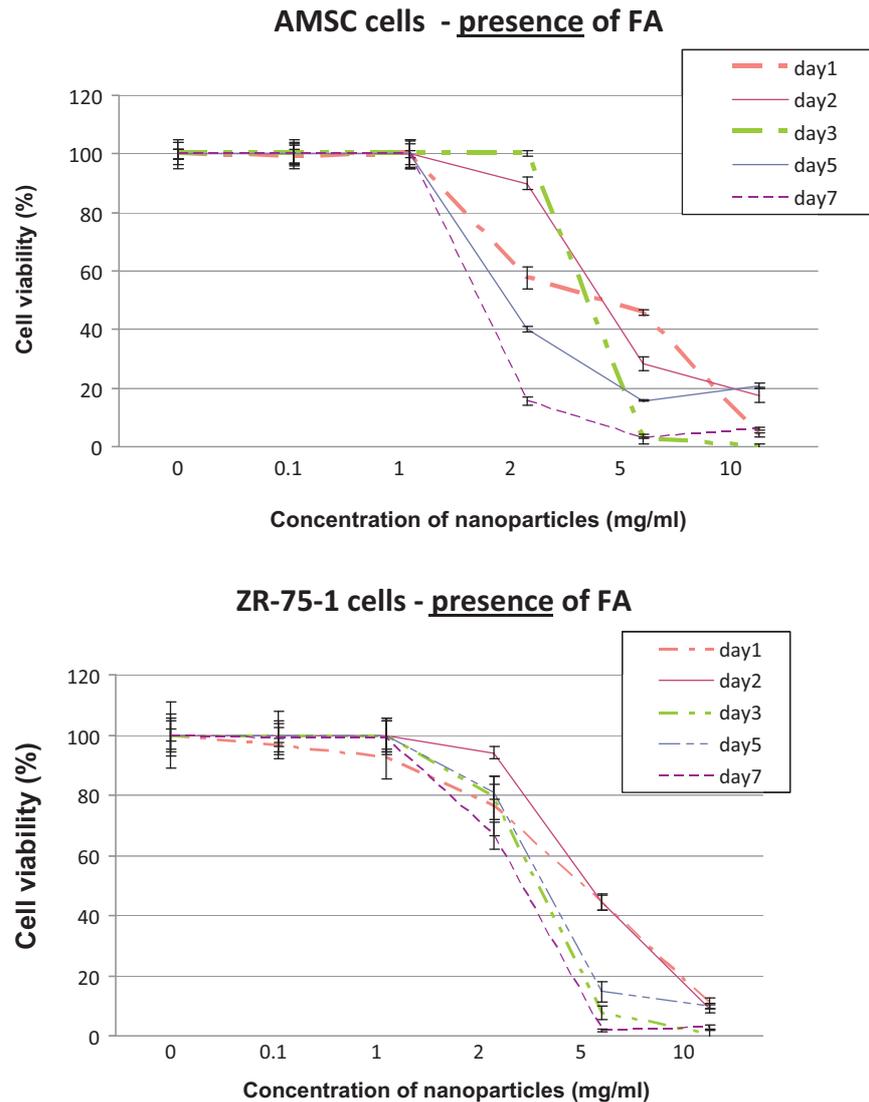## ZR-75-1 cells - <u>presence</u> of FA

Fig. 4. MTT cytotoxicity data for apatite-based colloids functionalized by FA, for AMSC and ZR-75-1 cells.

the 1 mg/ml value as the inflexion value for these colloids on AMSC cells.

Similar tests were also carried out on ZR-75-1 cancer cells (that do not overexpress folate receptors), and the data (Fig. 4) indicated that the inflexion of the cytotoxicity curve occurred in the range 1–2 mg/ml.

These findings point out the low cytotoxicity of these colloidal systems, at least for such cells which do not specifically respond to folic acid. These findings will be taken as reference for future works on these colloids. Additional experiments are in progress on cells that overexpress folate receptors.

3.1.3. Investigation of pro-inflammatory potential

The pro-inflammatory potential of the apatite colloidal nanoparticles prepared was investigated here by following their interaction with Human monocytes, via the evaluation of the amount of ROI produced by the cells (luminol-enhanced chemiluminescence).

Chemiluminescence measurements (Fig. 5), carried out after 1 h of contact between the colloidal nanoparticles (purified by dialysis and stabilized at physiological pH) and the monocytes, and for concentrations in nanoparticles between 0 and 120 µg/ml showed no significant effect (i.e. activator or inhibitor) on the production
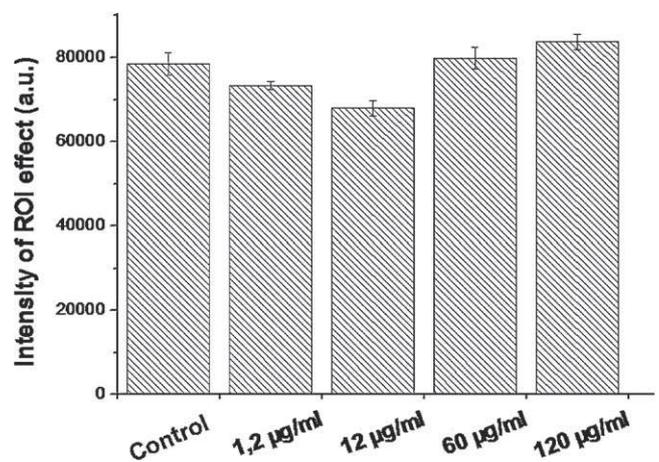

Fig. 5. Luminol-enhanced chemiluminescence intensity measurements for monocytes contacted with colloidal apatite nanoparticles (1 h contact time).
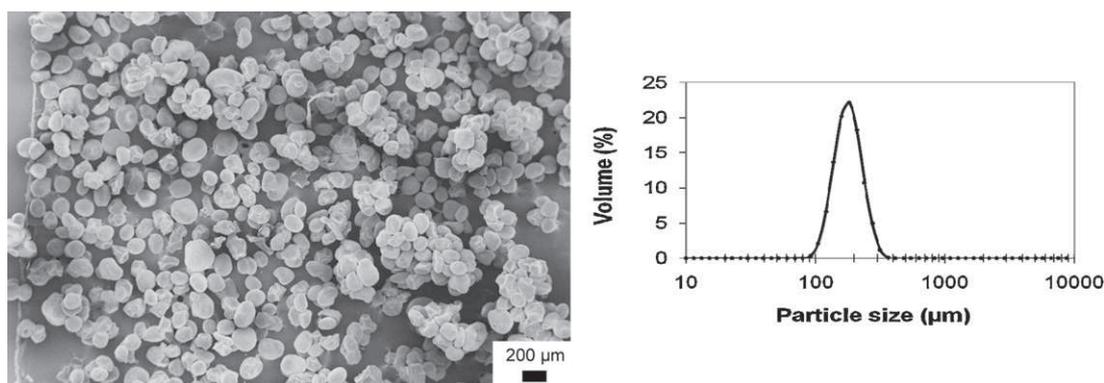
Fig. 6. SEM micrograph of LMAP microspheres loaded with erythrosin (ERY-LMAP) (initial magnification 200×), and particle size distribution according to laser light scattering measurements.

of ROI. These results indicate that the intrinsic pro-inflammatory potential of such colloids is low and remains undetectable after 1 h of contact.

3.1.4. Study of apatite colloidal nanoparticles internalization by ZR-75-1 breast cancer cells

This study was aimed at examining, in a preliminary approach, the possibilities of internalization of our colloidal nanoparticles by cells. For these tests, ZR-75-1 breast cancer cells were used. The concentration of nanoparticles in the culture medium was set to 1.5 mg/ml, with a contact time of 24 h at 37 °C. ICP-AES measurements were then carried out after cell washing, counting, and acidic treatment (see Section 2): the quantitative data obtained indicated that the Ca and Eu contents in the acidic aliquots increased after being contacted with the nanoparticles, leading to the ratio between the increase in Eu (initially absent of the cytoplasm) and the increase in Ca of $Eu/Ca = 0.088 \pm 0.002$ mass ratio. This value corresponds to a $Eu/(Ca + Eu)$ molar ratio of 0.022 ± 0.006, which is in perfect agreement with the $Eu/(Ca + Eu)$ molar ratio characteristic of the initial nanoparticles (2%).

Such results can be explained by the existence of a close interaction between the nanoparticles and the cells during the contacting time, leading to an internalization of the particles. Taking into account the small size of the particles (of the order of 30–40 nm), cell internalization through the endocytosis process appears as the most probable scenario, although this question will require further examination.

These first results confirm the possibility to use such nano-systems for biomedical applications requiring an intracellular action (either in terms of diagnosis or of therapeutics). Additional experiments are in progress with cells overexpressing folate receptors, so as to potentially evidence an increased internalization rate in the case of nanoparticles associated with folic acid.

Preliminary analyses by optical microscopy coupled with a spectrophotometer, carried out on air-dried colloids, have pointed out the europium signature of the particles by showing luminescence peaks around 590 and 615 nm (upon excitation at 365 nm). Additional experiments are now planned for investigating the possibility to detect the europium luminescence signature for cell-internalized particles.

3.2. Biomimetic apatite–pectin microspheres composites

In the following sections, we address the elaboration of new biomimetic apatite-based composite biomaterials involving LMAP microspheres as drug reservoirs distributed within the biomimetic apatite matrix.

3.2.1. Physico-chemical aspects

Generally speaking, the association of a drug with mineral bone repair scaffolds is not a straightforward task, in particular due to the relative fragility of the organic molecules (usually heat-sensitive) constituting the drug. The processing of scaffolds for bone engineering often requires heat treatments/sintering at high temperature. In these cases however, the drug/scaffold association can then only be considered as a subsequent step, after cooling, for example by filling (generally imperfectly) the accessible open porosity of the scaffold by immersion in a solution containing the drug, followed by drying steps. A better suited way for performing drug/scaffold associations can nonetheless be considered if the scaffold characteristics allow its preparation and processing without the use of elevated temperatures and/or the appliance of large mechanical pressures. In this view, along with their intrinsic biomimetism properties, nanocrystalline apatites then represent an interesting class of material due to the possibility to obtain robust biomaterials at low or ambient temperatures (Grossin et al., 2010) even without pressing procedures. As stated earlier, the possibility to associate a calcium phosphate cement (CPC) with drugs has been reported (Ruhe et al., 2005; Habraken et al., 2008; Girod-Fullana et al., 2010). However, the kinetics of cement hardening, inducing a hydrolysis reaction, as well as the apatite characteristics (apatite being the final state of hardened CPC) are generally modified by the amount and nature of additives in the system. Also, pH variations and exothermic effects often accompany the cement hardening process, which may also potentially alter some drugs.

In this study, we thus investigated the possibility to associate LMAP microspheres with a biomimetic apatite phase obtained by direct precipitation as a gel, without any heating or high pressure treatment in the processing route.

Pectin is a naturally occurring heterogeneous water-soluble polysaccharide which is found in the cell wall of most plants. It consists mainly of linearly connected α-(1,4)-D-galacturonic acid monosaccharide units that may be methyl-esterified or amidated to varying extents. Low methoxy (with a degree of esterification DE < 50%) pectins (LMPs) and LM amidated pectins (LMAPs) can gel with an "egg box" configuration in the presence of many divalent cations (Grant et al., 1973), allowing the formation of microspheres by ionotropic gelation, without any use of organic solvents and harsh ingredients. Pectin is biocompatible, biodegradable (Orhan et al., 2006) and has recently demonstrated its potential interest to be used in the surface modification of medical devices and materials (Morra et al., 2004; Ichibouji et al., 2008) and particularly bone implant nanocrystalline coatings (Kokkonen et al., 2007, 2008, 2010; Bussy et al., 2008).
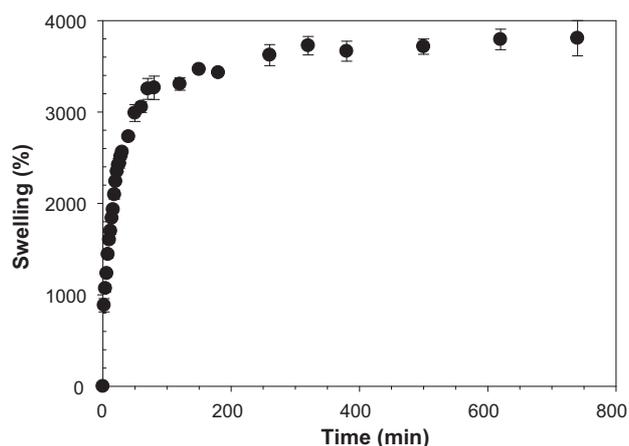
Fig. 7. Swelling properties of LMA-pectin microspheres loaded with erythrosine in SBF pH 7.25.

Fig. 8. (a) XRD patterns and (b) FTIR spectra for apatite–LMAP composites (3% and 18% LMAP) and for ceramic alone.

A LMAP with a DE of 30 and a degree of amidation (DA) of 19 was chosen, as we found it suitable for the elaboration of organic–mineral composites (Girod-Fullana et al., 2010).

As a first step, LMAP microspheres loaded with erythrosin B (ERY-LMAP) were prepared by ionotropic gelation in the presence of calcium ions. LMAP microspheres loaded with erythrosin B (ERY-LMAP) were obtained instantaneously when LMAP solutions were dropped into calcium bath. Intermolecular cross-links were formed between the negatively charged carboxyl groups of LMAP and the positively charged counter-ions, as previously described by Grant et al. (1973) in the "egg-box model". After drying, the resulting microspheres were characterized in terms of size distribution and morphology. Loaded LMAP microspheres with a weight average of volume distribution $D[4;3]$ of 195 μm were obtained, with monomodal and narrow particle size distribution (polydispersity index of 0.64) (Fig. 6). Microspheres appeared spherical to ovoid with a smooth surface when observed by SEM.

The swelling property of ERY-LMAP microspheres was then studied (Fig. 7). The weight gain raised sharply within the first 40 min until it reached a plateau. No downward trend in the curve, sign of microspheres erosion or degradation could be observed during the experiments. Once dried microspheres placed in aqueous media, high calcium chloride concentration entrapped in the microspheres exerted an osmosis phenomenon and water was absorbed, inducing swelling of the microspheres. Microspheres further stability can be explained by the strength of their network structure, due to the formation of stable interchain junction zones between each calcium ion and two carboxyl groups, reinforced by the presence of calcium ions in SBF.

Composite apatite–LMAP disks were obtained as detailed in Section 2. Gel drying carried out at 4 °C led, in our experimental conditions, to an amorphous compound as indicated by FTIR and XRD analyses (not shown). In contrast, an apatite phase was obtained upon drying at either 20, 37 or 50 °C as shown by XRD and FTIR analyses which pointed out apatite as the only crystallized phase in the system (Fig. 8). However, the dried composite disks obtained at 37 or 50 °C exhibited apparent flaws such as fracture lines (cracks) and these drying conditions were thus considered as inappropriate. These findings may probably be linked in these cases to a high drying rate, involving strong mechanical strains over short periods of time. In contrast, the composite disks obtained at RT (~20 °C) revealed an undamaged aspect and this drying temperature was then used for subsequent experiments. The volume decrease accompanying the drying step at RT was found to be of the order of 50%.
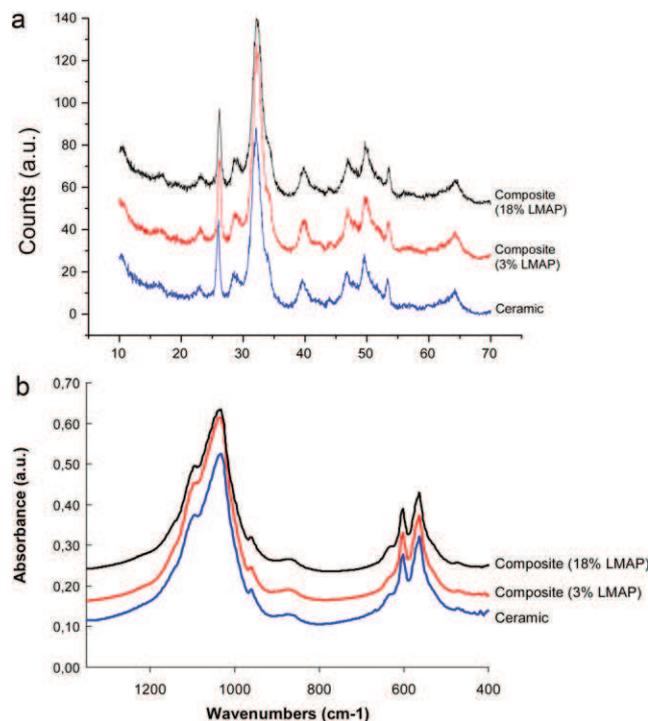
The presence of LMAP microspheres (introduced in varying amounts) dispersed within the apatite matrix was evidenced by optical microscopy imaging. Additionally, XRD and FTIR data showed that the physico-chemical characteristics of the apatite phase remained basically unchanged independently of the amount of LMAP microspheres associated to the mineral phase. Also, chemical analyses indicated that the Ca/P ratio of the apatite phase was essentially constant and close to 1.53 ± 0.04 (characteristic of non-stoichiometric biomimetic-like apatites) for LMAP w/w contents between 0% and 18% (corresponding to a mass of LMAP between 0 and 300 mg). These findings are particularly interesting as they show, contrarily to the cement processing route, that a single protocol can be set up for preparing various apatite–LMAP composites, where the amount of LMAP microspheres can be tailored as a function of the desired dose, regardless of the characteristics of the apatite phase that will remain unchanged. The upper limit of microspheres incorporation ratio into apatite is the consequence of their swelling properties and could be modulated by an accurate choice of pectin amidation and methoxylation degree. It was found to be about 10% (w/w) in the case of a pectin with a DA of 19% and DE of 30%.

It was thus interesting at this point to study the possibility to use these systems for a local drug delivery after implantation. In this view, using erythrosine as a model molecule, we investigated the release properties of the apatite matrix alone and of typical composite disks containing 6 and 9% (w/w) LMAP.

3.2.2. Release properties of apatite–LMAP microspheres composites

Composites *in vitro* drug release properties were evaluated for 1 week in SBF pH 7.25 at 37 °C, in order to mimic the ionic conditions encountered when implanted *in vivo* (Kokubo and Takadama, 2006). Erythrosin B was chosen as model drug because it is an anionic dye, fluorescein analog, presenting higher solubility at basic pH (it is a weak acid with a pK_a of 5.04), allowing us to study the release of a drug able to diffuse freely out of the composites without

Table 1
Kinetic analysis of erythrosin release from apatite–LMAP microspheres composites; comparison with LMAP microspheres and apatite reference.

	Cumulated erythrosin released within the first 24 h (%)	Cumulated erythrosin released after 7 days (%)	Higuchi model coefficient of determination r^2	Higuchi dissolution constant k_H ($\% \, h^{-1/2}$)
Apatite/ERY-LMAP 6%	6.43 ± 0.92	17.23 ± 0.67	0.994	1.358
Apatite/ERY-LMAP 9%	7.88 ± 0.74	20.13 ± 0.76	0.997	1.563
ERY-apatite	97.36 ± 2.63	100.06 ± 0.64	0.992	33.153
ERY-LMAP microspheres	50.04 ± 2.61	78.1 ± 0.98	0.923	9.711

presenting specific interactions with the apatite phase or LMAP. In our operating conditions, an encapsulation efficiency of 68% and a drug loading of 15% of erythrosin B into LMAP microspheres were obtained. Reaching better entrapment efficiency was not the purpose of our study, but it could be optimized by playing with the counter-ion type and concentration, with the pH of the cross-linking bathes and with the composition of the rinsing solutions before drying (Chambin et al., 2006). Dry ERY-LMAP microspheres were incorporated into the apatite matrix at weight ratios of 6% and 9%, leading to composites with an increasing drug loading. Release patterns were presented by plotting the cumulated percentage of erythrosin B released versus time.

Fig. 9 displays the release profiles of erythrosin B according to LMAP microspheres ratio into the composites. They were almost identical in shape, presenting a very limited initial burst in the initial 24 h (see Table 1) followed by a slow and sustained drug release. The release data were simulated using Higuchi theory which investigated whether the erythrosin B cumulative release percentages from composites were proportional to the square root of time. They correlated well with this model, suggesting that erythrosin B was released by Fickian diffusion from all the composites during the experiments.

Releases of similar levels of erythrosin B release from a pure apatite compound (so-called "ceramic") and from LMAP microspheres were compared under the same experimental conditions (Fig. 9). While the pure apatite sample released 100% erythrosin B within 24 h, clearly showing that there is no interaction between the apatite phase and the dye, the composite and microspheres release patterns were sustained, demonstrating the role of LMAP microspheres in controlling drug diffusion (Table 1). Such sustained release can be explained by LMAP microspheres sensitivity to ionic conditions. They behave as hydrophilic matrices whose release ability is currently related to their swelling ability in dissolution
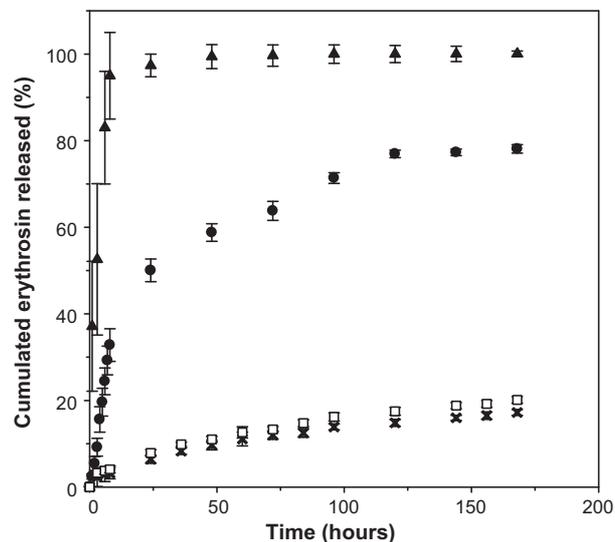
Fig. 9. Erythrosin *in vitro* release from apatite–LMAP microspheres composites in SBF pH 7.25 at 37 °C (×: apatite/ERY-LMAP 6% composite; □: apatite/ERY-LMAP9% composite; ●: ERY-LMAP microspheres; ▲: ERY-apatite).

media (Chambin et al., 2006). The presence of calcium in the LMAP surrounding has been shown to enhance cross-linking and aggregation of the pectin chains (Sriamornsak, 1999). In our case, LMAP microspheres are immersed in SBF medium, which contain calcium ions, and surrounded by apatite in the case of composites, thus swelling patterns and subsequently drug release were limited for microspheres and composites, in a greater extent for the latter. Steric constraints might also have hindered microspheres swelling within the composites. Additional drug diffusion through
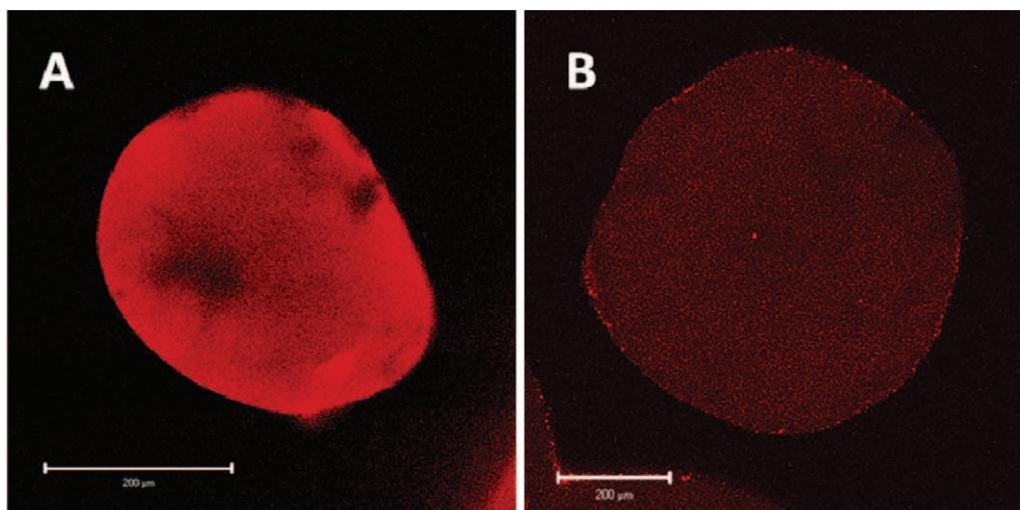
Fig. 10. Fluorescence confocal microscopy photographs of cross sections of LMA-pectin microspheres loaded with erythrosine, retrieved from the surface of the composites (a) before release experiments (D0); (b) after 7 days of immersion in SBF pH 7.25 at 37 °C (D7).

the apatite porosity, some of them being partially blocked by LMAP microspheres, could also explain this slowing down, whereas no differences could be observed between the two LMAP ratios tested during our experiments.

Although these results have to be completed by longer release studies, they yet clearly show the interest of combining nanocrystalline apatite with LMAP microspheres to generate tailored drug delivery systems with improved drug release properties.

After 1 week of release, LMAP microspheres were still intact and could be retrieved from the bioceramic and observed by confocal laser microscopy. Confocal fluorescence observation (Fig. 10) confirmed incorporated microspheres integrity and moderate swelling after a week of immersion in SBF. Erythrosin B distribution within the microspheres and progressive diminution over time were observable, even more clearly on microspheres located near the periphery of the composites. A homogenous distribution of the dye within the microspheres at day 0 (D0, Fig. 10a) and a fluorescence diminution from the center to the outer of the particles at D7 confirmed a diffusion release mechanism.

These results are promising and illustrate the potential interest of nanocrystalline ceramics in elaborating innovative drug release systems that could find application in bone cancer therapy.

4. Conclusions

The data reported in this contribution enabled us to propose and test novel approaches for the preparation, storage and processing of biomimetic-apatite-based nanosystems produced in view of cancer-related applications.

We showed first that hybrid luminescent colloidal nanoparticles based on the association of Eu-doped biomimetic apatite nanocrystals, a phospho-lipid moiety (AEP) and also possibly vitamin B9 (folic acid, a potential cell-targeting agent) exhibited a low cytotoxicity and pro-inflammatory potential and could be internalized by ZR-75-1 breast cancer cells. These findings then allow one to envision potential applications in intracellular imaging by luminescence, which will be addressed in future works.

In a second type of approach, the incorporation of LMA pectin microspheres within a nanocrystalline apatite matrix led to organic–mineral composites with original properties. Interestingly, the presence and amount of pectin microspheres did not modify the physico-chemical characteristics of the apatite phase. In terms of drug delivery, sustained release of our model molecule was obtained, whereas it developed no specific interaction with apatite nor pectin. The presence of LMAP appeared as a parameter contributing to regulate drug diffusion. By adjusting their pectin microspheres content, it should be possible to design tailorable composites whose release rates could be controlled upon demand. To our knowledge no previous studies concerning nanocrystalline apatite-polymer microspheres composite materials had been published previously.

These results add to the existing literature on synthetic biomimetic nano-systems, by exploring these novel options in the field of cancer diagnosis and treatment.

Acknowledgements

References

Al-Kattan, A., Dufour, P., Dexpert-Ghys, J., Drouet, C., 2010. Preparation and physico-chemical characteristics of luminescent apatite-based colloids. J. Phys. Chem. C 114, 2918–2924.

Antony, A.C., 1992. The biological chemistry of folate receptors. Blood 79, 2807–2820.

Atyabi, F., Majzoob, S., Iman, M., Salehi, M., Dorkoosh, F., 2005. In vitro evaluation and modification of pectinate gel beads containing trimethyl chitosan, as a multi-particulate system for delivery of water-soluble macromolecules to colon. Carbohydr. Polym. 61, 39–51.

Autefage, H., Briand-Mesange, F., Cazalbou, S., Drouet, C., Combes, C., Swider, P., Rey, C., 2009. Adsorption and release of BMP-2 on nanocrystalline apatite-coated and uncoated hydroxyapatite/beta-tricalcium phosphate porous ceramics. J. Biomed. Mater. Res. B 91, 706–715.

Barroug, A., Kuhn, L.T., Gerstenfeld, L.C., Glimcher, M.J., 2004. Interactions of cisplatin with calcium phosphate nanoparticles: in vitro controlled adsorption and release. J. Orthop. Res. 22, 703–708.

Bouladjine, A., Al-Kattan, A., Dufour, P., Drouet, C., 2009. New advances in nanocrystalline apatite colloids intended for cellular drug delivery. Langmuir 25, 12256–12265.

Boyer, L., Piriou, B., Carpena, J., Lacout, J.L., 2000. Study of sites occupation and chemical environment of Eu^{3+} in phosphate-silicates oxyapatites by luminescence. J. Alloys Compd. 311, 143–152.

Bruchez, M., Moronne, M., Gin, P., Weiss, S., Alivisatos, A.P., 1998. Semiconductor nanocrystals as fluorescent biological labels. Science 281, 2013–2016.

Bussy, C., Verhoef, R., Haeger, A., Morra, M., Duval, J.L., Vigneron, P., Bensoussan, A., Velzenberger, E., Cascardo, G., Cassinelli, C., Schols, H., Knox, J.P., Nagel, M.D., 2008. Modulating in vitro bone cell and macrophage behavior by immobilized enzymatically tailored pectins. J. Biomed. Mater. Res. A 86, 597–606.

Cazalbou, S., Eichert, D., Ranz, X., Drouet, C., Combes, C., Harmand, M.F., Rey, C., 2005. Ion exchanges in apatites for biomedical applications. J. Mater. Sci.: Mater. Med. 16, 405–409.

Chambin, O., Dupuis, G., Champion, D., Voilley, A., Pourcelot, Y., 2006. Colon-specific drug delivery: influence of solution reticulation properties upon pectin beads performance. Int. J. Pharm. 321, 86–93.

Couvreur, P., Gref, R., Andrieux, K., Malvy, C., 2006. Nanotechnologies for drug delivery: application to cancer and autoimmune diseases. Prog. Solid State Chem. 34, 231–235.

Drouet, C., Carayon, M.T., Combes, C., Rey, C., 2008. Surface enrichment of biomimetic apatites with biologically active ions Mg^{2+} and Sr^{2+}: a preamble to the activation of bone repair materials. Mater. Sci. Eng. C 28, 1544–1550.

Drouet, C., Bosc, F., Banu, M., Largeot, C., Combes, C., Dechambre, G., Estournes, C., Raimbeaux, G., Rey, C., 2009. Nanocrystalline apatites: from powders to biomaterials. Powder Technol. 190, 118–122.

Fizet, J., Riviere, C., Bridot, J.L., Charvet, N., Louis, C., Billotey, C., Raccurt, M., Morel, G., Roux, S., Perriat, P., Tillement, O., 2009. Multi-luminescent hybrid gadolinium oxide nanoparticles as potential cell labeling. J. Nanosci. Nanotechnol. 9, 5717–5725.

Gautier, H., Chamblain, V., Weiss, P., Merle, C., Bouler, J.M., 2010. In vitro characterisation of calcium phosphate biomaterials loaded with lidocaine hydrochloride and morphine hydrochloride. J. Mater. Sci.: Mater. Med. 21, 3141–3150.

Girod-Fullana, S., Ternet, H., Freche, M., Lacout, J.L., Rodriguez, F., 2010. Controlled release properties and final macroporosity of a pectin microspheres–calcium phosphate composite bone cement. Acta Biomater. 6, 2294–2300.

Grant, G.T., Morris, E.R., Rees, D.A., Smith, P.J.C., Thom., D., 1973. Biological interactions between polysaccharides and divalent cations: the egg-box model. FEBS Lett. 32, 195–198.

Grossin, D., Rollin-Martinet, S., Estournes, C., Rossignol, F., Champion, E., Combes, C., Rey, C., Chevallier, G., Drouet, C., 2010. Biomimetic apatite sintered at very low temperature by Spark Plasma Sintering (SPS): physico-chemistry and microstructure aspects. Acta Biomater. 6, 577–585.

Habraken, W.J.E.M., Boerman, O.C., Wolke, J.G.C., Mikos, A.G., Jansen, J.A., 2008. In vitro growth factor release from injectable calcium phosphate cements containing gelatin microspheres. J. Biomed. Mater. Res. A 91, 614–622.

Ichibouji, T., Miyazaki, T., Ishida, E., Ashizuka, M., Sugino, A., Ohtsuki, C., Kuramoto, K., 2008. Evaluation of apatite-forming ability and mechanical property of pectin hydrogels. J. Ceram. Soc. Jpn. 116, 74–78.

Josse, S., Faucheux, C., Soueidan, A., Grimandi, G., Massiot, D., Alonso, B., Janvier, P., Laib, S., Pilet, P., Gauthier, O., Daculsi, G., Guicheux, J., Bujoli, B., Bouler, J.M., 2005. Novel biomaterials for bisphosphonate delivery. Biomaterials 26, 2073–2080.

Kamen, B.A., Wang, M., Streckfuss, A.J., Peryea, X., Anderson, R.G., 1988. Delivery of folates to the cytoplasm of MA 104 cells is mediated by a surface-membrane receptor that recycles. J. Biol. Chem. 263, 13602–13609.

Kokkonen, H.E., Ilvesaro, J.M., Morra, M., Schols, H.A., Tuukkanen, J., 2007. Effect of modified pectin molecules on the growth of bone cells. Biomacromolecules 8, 509–515.

Kokkonen, H., Cassinelli, C., Verhoef, R., Morra, M., Schols, H.A., Tuukkanen, J., 2008. Differentiation of osteoblasts on pectin-coated titanium. Biomacromolecules 9, 2369–2376.

Kokkonen, H., Niiranen, H., Schols, H.A., Morra, M., Stenback, F., Tuukkanen, J., 2010. Pectin-coated titanium implants are well-tolerated in vivo. J. Biomed. Mater. Res. A 93, 1404–1409.

Kokubo, T., Takadama, H., 2006. How useful is SBF in predicting in vivo bone bioactivity? Biomaterials 27, 2907–2915.

Laskin, D.L., Laskin, J.D., 2001. Role of macrophages and inflammatory mediators in chemically induced toxicity. Toxicology 160, 111–118.

Lebugle, A., Rodrigues, A., Bonnevialle, P., Voigt, J.J., Canal, P., Rodriguez, F., 2002. Study of implantable calcium phosphate systems for the slow release of methotrexate. Biomaterials 23, 3517–3522.

Lefevre, L., Gales, A., Olagnier, D., Bernad, J., Perez, L., Burcelin, R., Valentin, A., Auwerx, J., Pipy, B., Coste, A., 2010. PPARgamma ligands switched high fat diet-induced macrophage M2b polarization toward M2a thereby improving intestinal Candida elimination. PLoS One 5, e12828.

LeGeros, R.Z., 2008. Calcium phosphate-based osteoinductive materials. Chem. Rev. 108, 4742–4753.

Moghimi, S.M., Bonnemain, B., 1999. Subcutaneous and intravenous delivery of diagnostic agents to the lymphatic system: applications in lymphoscintigraphy and indirect lymphography. Adv. Drug Deliv. Rev. 37, 295–312.

Moghimi, S.M., Hunter, A.C., Murray, J.C., 2001. Long-circulating and target-specific nanoparticles: theory to practice. Pharmacol. Rev. 53, 283–318.

Mondejar, S.P., Kovtun, A., Epple, M., 2007. Lanthanide-doped calcium phosphate nanoparticles with high internal crystallinity and with a shell of DNA as fluorescent probes in cell experiments. J. Mater. Chem. 17, 4153–4159.

Morra, M., Cassinelli, C., Cascardo, G., Nagel, M.D., Della Volpe, C., Siboni, S., Maniglio, D., Brugnara, M., Ceccone, G., Schols, H.A., Ulvskov, P., 2004. Effects on interfacial properties and cell adhesion of surface modification by pectic hairy regions. Biomacromolecules 5, 2094–2104.

Orhan, Z., Cevher, E., Mulazimoglu, L., Gurcan, D., Alper, M., Araman, A., Ozsoy, Y., 2006. The preparation of ciprofloxacin hydrochloride-loaded chitosan and pectin microspheres – their evaluation in an animal osteomyelitis model. J. Bone Joint Surg.: Br. 88B, 270–275.

Ow, H., Larson, D.R., Srivastava, M., Baird, B.A., Webb, W.W., Weisner, U., 2005. Nano Lett. 5, 113–117.

Parak, W.J., Gerion, D., Pellegrino, T., Zanchet, D., Micheel, C., Williams, S.C., Boudreau, R., Le Gros, M.A., Larabel, C.A., Alivisatos, A.P., 2003. Biological applications of colloidal nanocrystals. Nanotechnology 14, R15–R17.

Parker, N., Turk, M., Westrick, E., Lewis, J., Low, P.S., Leamon, C.P., 2005. Folate receptor expression in carcinomas and normal tissues determined by a quantitative radioligand binding assay. Anal. Biochem. 338, 284–293.

Rey, C., Combes, C., Drouet, C., Sfihi, H., Barroug, A., 2007. Physico-chemical properties of nanocrystalline apatites: implications for biominerals and biomaterials. Mater. Sci. Eng. C 27, 198–205.

Rey, C., Combes, C., Drouet, C., Glimcher, M.J., 2009. Bone mineral: update on chemical composition and structure. Osteoporos. Int. 20, 1013–1021.

Roveri, N., Palazzo, B., Iafisco, M., 2008. The role of biomimetism in developing nanostructured inorganic matrices for drug delivery. Expert Opin. Drug Deliv. 5, 861–877.

Ruhe, P.Q., Boerman, O.C., Russel, F.G.M., Spauwen, P.H.M., Mikos, A.G., Jansen, J.A., 2005. Controlled release of rhBMP-2 loaded poly(DL-lactic-co-glycolic acid)/calcium phosphate cement composites in vivo. J. Control. Release 106, 162–171.

Saha, S.K., Banerjee, A., Banerjee, S., Bose, S., 2009. Synthesis of nanocrystalline hydroxyapatite using surfactant template systems: role of templates in controlling morphology. Mater. Sci. Eng. C 29, 2294–2301.

Schroeder, J.E., Shweky, I., Shmeeda, H., Banin, U., Gabizon, A., 2007. Folate-mediated tumor cell uptake of quantum dots entrapped in lipid nanoparticles. J. Control. Release 124, 28–34.

Spinella, M.J., Brigle, K.E., Sierra, E.E., Goldman, I.D., 1995. Distinguishing between folate-receptor-alpha-mediated transport and reduced-folate-carrier-mediated transport in L1210 leukemia cells. J. Biol. Chem. 270, 7842–7849.

Sriamornsak, P., 1999. Effect of calcium concentration, hardening agent and drying condition on release characteristics of oral proteins from calcium pectinate gel beads. Eur. J. Pharm. Sci. 8, 221–227.

Tran, P.A., Zhang, L.J., Webster, T.J., 2009. Carbon nanofibers and carbon nanotubes in regenerative medicine. Adv. Drug Deliv. Rev. 61, 1097–1114.